PHILOSOPHICAL TRANSACTIONS OF THE ROYAL SOCIETY A MATHEMATICAL, PHYSICAL & ENGINEERING SCIENCES

The Gas Dynamics of Massive Evaporation and Condensation

P. N. Shankar and M. D. Deshpande

Phil. Trans. R. Soc. Lond. A 1991 **335**, 487-511
doi: 10.1098/rsta.1991.0058

The gas dynamics of massive evaporation and condensation

By P. N. Shankar and M. D. Deshpande

Computational and Theoretical Fluid Dynamics Division, National Aeronautical Laboratory, Bangalore 560 017, India

Contents

	PAGE
1. Introduction	488
2. Formulation of the gas dynamic problem	489
3. The inviscid problem and solution	490
4. The viscous solution: Prandtl number = 0.75	495
4.1. The solution for small heights ($\tilde{\delta}/\tilde{H} \to \infty$)	501
4.2. Asymptotic analysis for large heights ($\tilde{\delta}/\tilde{H} \to 0$)	502
5. The viscous solution for arbitrary Prandtl number	505
6. Discussion	507
7. Conclusion	510
References	510

We consider in this paper the gas dynamic field associated with liquid-vapour phase change between two parallel liquid surfaces. The full nonlinear equations for a compressible, viscous, heat conducting gas are considered with no limitations on the Mach number. First the inviscid problem is formulated and the exact solutions found for the temperature and velocity fields. While these solutions are qualitatively similar to those found using linearized analyses significant quantitative differences exist, especially at higher mass fluxes. Next the nonlinear, viscous field is obtained for a vapour with a Prandtl number of 0.75, as the equations simplify for this case. The results obtained show dramatic departures from the inviscid solutions: the temperature profiles, which may no longer be monotonic, can manifest both undershoots and overshoots. Cases exist, whose relevance to the phase change problem is yet to be established, where the overshoot is many times the applied temperature difference. Asymptotic solutions are also developed for small and large values of the height parameter $\tilde{\delta}/\tilde{H}$ which show interesting features; for small heights the temperature profile is, surprisingly, quadratic in y while for large heights the flow field is uniform with boundary layers at both surfaces. The restriction on the Prandtl number is then removed. The solutions for arbitrary Prandtl number are shown to merge smoothly to the appropriate inviscid solution as $Pr \to 0$. These solutions also show that $Pr = \frac{3}{4}$ is a very good approximation for most gases and vapours of interest.

The remarkable predictions that have been made here show that the role of viscosity in the gas dynamic field in liquid vapour phase change has so far been vastly underestimated. The present results will necessitate serious rethinking on the inviscid, linearized theoretical framework that has so far, by and large, been used.

Phil. Trans. R. Soc. Lond. A (1991) **335**, 487–511
Printed in Great Britain

These results will also have a serious bearing on any future experimental investigations of the phenomenon.

1. Introduction

Even though the phenomena of evaporation and condensation are so common in nature and have been studied extensively, there are many aspects to them that are still poorly understood. Part of the difficulty stems from the fact that it is difficult to conduct simple, unambiguous experiments in surroundings which permit chemical purity of the liquid and vapour. On the other hand, theoretical analysis needs to overcome the hurdle posed by the fact that the problem is naturally posed only for the velocity distribution function: thus either the Boltzmann equation or the continuum equations coupled to appropriate Knudsen layers have to be solved. As a consequence most analyses have been limited to the linearized low Mach number case. We might also point out that a serious limitation so far has been our poor understanding of the nature of the liquid–vapour interfaces. These have had to be modelled in a possibly over simplified manner. Another issue that has been ignored so far, and to which we here address ourselves, is that of the roles of viscosity and nonlinearity in the gas dynamic field especially for large mass fluxes. It will be seen that their effects can be very striking indeed.

Plesset (1952) was perhaps the first to attempt to compute, in the absence of any contaminant, the evaporative mass flux between two pure liquid surfaces at different temperatures (see figure 1). The one-dimensional continuum equations hold in the bulk of the fluid; for low Mach numbers, ignoring viscosity, these were solved and coupled to separate analyses of the Knudsen layers to yield a result for the mass flux. While the basic idea both in this work and in Plesset & Prosperetti (1976) was correct the mass flux and the temperature field were incorrectly computed because the temperature was assumed to be continuous at the liquid–vapour interfaces. It was Pao (1971) who made the remarkable discovery, by solving the linearized Boltzmann equation for the vapour, that in general the temperature suffered large jumps at the interfaces; jumps that could, in principle, be large enough for the temperature gradient in the vapour to oppose the applied temperature gradient. Although this surprising result has since been confirmed for the plane geometry (Matsushita 1976; Aoki & Cercignani 1983), for polyatomic molecules and gas mixtures (Cercignani *et al.* 1985; Shankar 1988) and for the spherical geometry (implied in Shankar (1970) and in Onishi (1986)), it still remains controversial. For example Koffman *et al.* (1984) have even suggested that the inverted temperature profile casts a shadow of doubt on the fundamental theory. Although an experimental verification would seem of crucial importance and has, indeed, been suggested a number of times, the only experimental study available seems to be that of Shankar & Deshpande (1990*a*). Using mercury as a working fluid they were able to establish the existence of large temperature jumps at the interfaces; however, they were unable to conclusively establish the existence or non-existence of the inverted temperature profile.

The aim of the present study is to explore an aspect that has so far been neglected: the role of viscosity and nonlinearity in the phase change phenomenon. It has always been assumed, principally because attention has been limited to small mass fluxes, that viscous normal stresses and dissipation would play insignificant roles; in a sense this was inconsistent since thermal conductivity was always included. Referring to figure 1, our attention will be limited to the gas dynamic field between the hot and

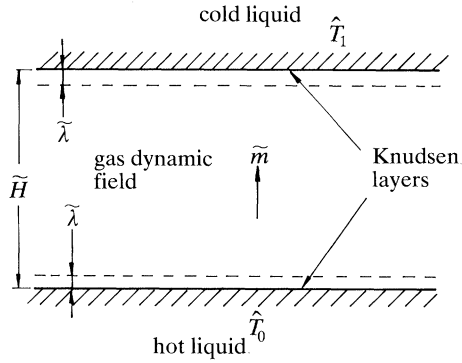

Figure 1. The gas dynamic field between an evaporating liquid surface and a condensing liquid surface.

cold liquid surfaces, outside the Knudsen layers which are restricted to distances of the order of a mean free path, $\tilde{\lambda}$, adjoining the liquid surfaces; naturally, we are interested in the continuum régime with $\tilde{\lambda}$ very much smaller than the distance $\tilde{H}$ between the surfaces. We emphasize that we will not be concerned with the Knudsen layers or with solving the complete phase change problem; this will permit us to clearly separate out and identify the role played in the phenomenon by convection and dissipation in the continuum field. Initially our interest was motivated by certain features of the temperature field found in our experimental results. We have since found that the viscous effects at high mass fluxes are remarkable in their own right and appear to be of very general interest.

Before proceeding with the formulation and analysis of this problem it may be pertinent to point out its relationship to the problem of the determination of shock structure based on the Navier–Stokes equations (see, for example, Morduchow & Libby 1949; von Mises 1950). No doubt, the one-dimensional gas dynamic equations for a compressible, viscous, heat conducting fluid hold in either case. However, two crucial differences arise, namely, the boundary conditions are different and the interval is finite as opposed to infinite. These lead to strikingly different phenomena.

2. Formulation of the gas dynamic problem

It will prove convenient to normalize all lengths by $\tilde{H}$, the distance between the liquid surfaces (see figure 1). In what follows the subscripts 0 and 1 will refer to the conditions of the vapour (or gas) at the lower and upper surfaces respectively. Then all the gas dynamic field quantities will be normalized by $\tilde{v}_0$, $\tilde{\rho}_0$, $\tilde{p}_0$ and $\tilde{T}_0$ the lower velocity, density, pressure and temperature respectively. With this chosen non-dimensionalization, the steady, one-dimensional gas dynamic equations for a compressible, viscous, heat conducting fluid take the form

$$\rho v = 1, \tag{1.1}$$

$$\frac{\mathrm{d}v}{\mathrm{d}y} = -\frac{1}{\gamma M_0^2}\frac{\mathrm{d}p}{\mathrm{d}y} + \frac{4}{3}\frac{1}{Re}\frac{\mathrm{d}^2 v}{\mathrm{d}y^2}, \tag{1.2}$$

$$\frac{\mathrm{d}T}{\mathrm{d}y} = \frac{(\gamma-1)}{\gamma} v\frac{\mathrm{d}p}{\mathrm{d}y} + \left(\frac{\tilde{\delta}}{\tilde{H}}\right)\frac{\mathrm{d}^2 T}{\mathrm{d}y^2} + \frac{4}{3}\left(\frac{\tilde{\delta}}{\tilde{H}}\right)(\gamma-1)\,Pr M_0^2\left(\frac{\mathrm{d}v}{\mathrm{d}y}\right)^2, \tag{1.3}$$

$$p = \rho T. \tag{1.4}$$

PHILOSOPHICAL TRANSACTIONS OF THE ROYAL SOCIETY A MATHEMATICAL, PHYSICAL & ENGINEERING SCIENCES

It may be observed from the above that the dynamic and thermodynamic properties of the fluid such as viscosity $\tilde{\mu}$, thermal conductivity $\tilde{k}$, specific heat $\tilde{c}_p$, etc., have been assumed to be constants; the equation of state has also been assumed to correspond to that of a perfect gas. These assumptions are all quite reasonable for the situations, far from the critical point, of interest to us. The equations above contain, apart from the specific heat ratio γ, four dimensionless parameters

$Re = (\tilde{\rho}_0 \tilde{v}_0 \tilde{H})/\tilde{\mu}$, the Reynolds number;

$M = \tilde{v}/\tilde{c}$, the Mach number;

$\tilde{\delta}/\tilde{H} = \tilde{k}/(\tilde{m}\tilde{c}_p \tilde{H})$, the height parameter based on the thermal boundary layer thickness;

$Pr = \tilde{\mu}\tilde{c}_p/\tilde{k}$, the Prandtl number,

where $\tilde{m}$ is the mass flux and $\tilde{c}$ is the sound speed.

It may be noted that while the thermal boundary layer thickness $\tilde{\delta}$ has played an important role in earlier investigations (see, for example, Aoki & Cercignani 1983), the Mach number, Reynolds number and Prandtl number have appeared infrequently, if at all. The following relationship between $\tilde{\delta}/\tilde{H}$, Re and Pr

$$Re = (Pr\,\tilde{\delta}/\tilde{H})^{-1} \tag{2}$$

should also be noted. For the setting of the present investigation it appears more natural to deal with $\tilde{\delta}/\tilde{H}$ and Pr and hence we will primarily refer to these quantities alone with the understanding that the Reynolds number can be computed from (2) above.

Regarding the boundary conditions, we first observe that the interval of interest now lies in $0 \leqslant y \leqslant 1$. All the vapour field properties are now assumed given at the lower surface i.e. $v_0 = T_0 = \rho_0 = 1$ and M_0 (and Re) are given. For the general viscous case two conditions then need to be specified at the top surface e.g. p_1 and T_1 may be given. For the inviscid case corresponding to $Pr = 0$, however, only one condition can be specified, e.g. T_1 or p_1; here we shall take T_1 to be given in this case.

In summary we see that, in addition to γ, the problem is fully specified by five other non-dimensional parameters: $\tilde{\delta}/\tilde{H}$, M_0, Pr, p_1 and T_1. We shall in what follows find that these six parameters span a very rich and intriguing variety of flow phenomena. Note that if the bulk viscosity $\tilde{\mu}_B$ of the vapour is not insignificant the present analysis will still be valid provided that the viscosity $\tilde{\mu}$ is enhanced by $0.75\tilde{\mu}_B$; no other change is necessary. It should also be pointed out that though this study has been motivated by the phase change phenomenon, the equations and boundary conditions considered refer to a very general gas-dynamic setting. Hence the formulation and results should be of considerable interest to the fluid dynamic community at large.

3. The inviscid problem and solution

We shall first consider the situation where the gas (a term which will from now on refer to gas or vapour) is assumed to be inviscid. While this assumption has been made either explicitly or implicitly, almost universally for the phase change problem, the thermal conductivity has always been retained. On the surface it may seem inconsistent to treat an inviscid fluid as heat conducting. It becomes clear on more

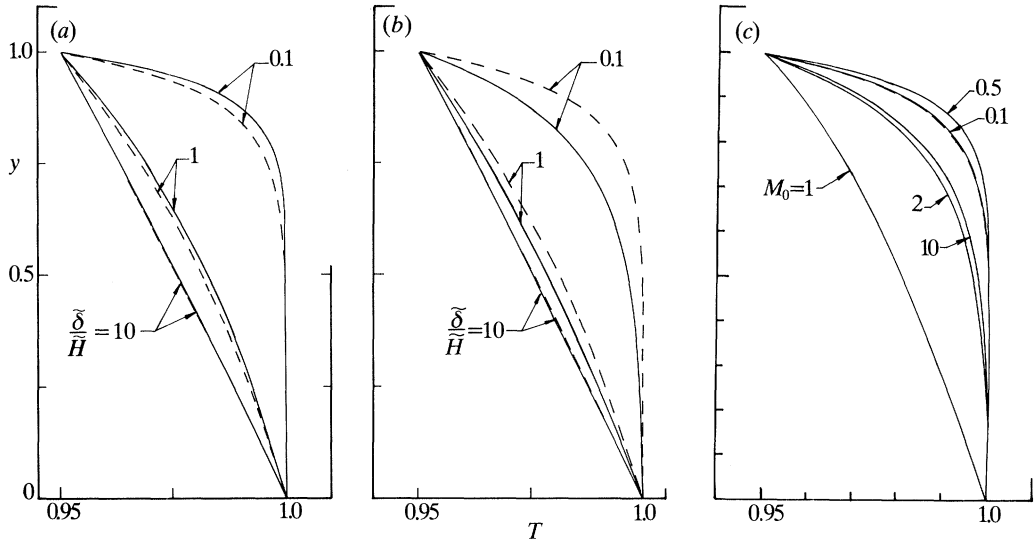

Figure 2. (*a*) The temperature profile as a function of $\tilde{\delta}/\tilde{H}$ for a Mach number $M_0 = 0.5$, $T_1 = 0.95$. (*b*) The temperature profile as a function of $\tilde{\delta}/\tilde{H}$ for a Mach number $M_0 = 2.0$, $T_1 = 0.95$. (*c*) The effect of Mach number for a fixed $\tilde{\delta}/\tilde{H} = 0.1$ and comparison with the exponential profile. (*a*)–(*c*); ----, Exponential.

careful scrutiny, however, that while at low Mach numbers viscous dissipation and viscous normal stress effects are likely to be inconsequential, thermal conduction cannot be ignored; in fact, at very low speeds energy transport takes place almost entirely by conduction. Thus this type of 'inviscid' model, while inconsistent for higher Mach numbers, is likely to be relevant to situations involving sufficiently low mass fluxes.

The governing equations can now be obtained by setting $Re = \infty$ and $Pr = 0$ in equations (1.2) and (1.3) which reduce to

$$\frac{\mathrm{d}v}{\mathrm{d}y} = -\frac{1}{\gamma M_0^2}\frac{\mathrm{d}p}{\mathrm{d}y}, \tag{3.1}$$

$$\frac{\mathrm{d}T}{\mathrm{d}y} = \frac{(\gamma-1)}{\gamma} v\frac{\mathrm{d}p}{\mathrm{d}y} + \left(\frac{\tilde{\delta}}{\tilde{H}}\right)\frac{\mathrm{d}^2T}{\mathrm{d}y^2}. \tag{3.2}$$

As regards boundary conditions, all the fluid properties are prescribed at the lower surface while the temperature alone is prescribed at the upper surface, i.e.

$$\rho = v = p = T = 1 \quad \text{at} \quad y = 0, \tag{4.1}$$

$$T = T_1 = \tilde{T}_1/\tilde{T}_0 \quad \text{at} \quad y = 1. \tag{4.2}$$

The momentum equation integrates immediately to

$$v + (1/\gamma M_0^2)\, p = B_i^* = 1 + 1/\gamma M_0^2, \tag{5}$$

where the constant B_i^* is the non-dimensional 'total momentum flux'. Using (1.1) and (1.4) to eliminate p in (5), we obtain an expression for the velocity

$$v = \begin{cases} 0.5[B_i^* - \sqrt{(B_i^{*2} - 4T/\gamma M_0^2)}], & \text{if} \quad M_0 < 1/\sqrt{\gamma}, \\ 0.5[B_i^* + \sqrt{(B_i^{*2} - 4T/\gamma M_0^2)}], & \text{if} \quad M_0 > 1/\sqrt{\gamma}, \end{cases} \tag{6}$$

which clearly indicates a critical Mach number equal to $1/\sqrt{\gamma}$, a point to which we will return later. If we substitute for the pressure from (3.1), the energy equation (3.2) can be integrated once to yield

$$T = -\tfrac{1}{2}(\gamma-1)M_0^2 v^2 + (\tilde{\delta}/\tilde{H})\,\mathrm{d}T/\mathrm{d}y + A_i^*, \tag{7}$$

where the constant A_i^* is, by the boundary conditions related to the slope of the temperature at the lower surface by

$$A_i^* = 1 + \tfrac{1}{2}(\gamma-1)M_0^2 - (\tilde{\delta}/\tilde{H})\,(\mathrm{d}T/\mathrm{d}y)_0. \tag{8}$$

We can now eliminate v from (7) to obtain a single nonlinear equation for the temperature. If we define

$$z = \sqrt{(B_i^{*2} - 4T/\gamma M_0^2)}, \tag{9}$$

z has to satisfy

$$z\frac{\mathrm{d}z}{\mathrm{d}y} = \frac{(\gamma+1)}{4\gamma(\tilde{\delta}/\tilde{H})}\left\{z^2 \pm \frac{2(\gamma-1)}{(\gamma+1)}B_i^* z + \left(\frac{8A_i^*}{(\gamma+1)M_0^2} - \frac{(3\gamma-1)}{(\gamma+1)}B_i^{*2}\right)\right\}, \tag{10}$$

where the $\{\pm\}$ sign is chosen as $M_0 \lesseqgtr 1/\sqrt{\gamma}$. The exact solution for $T(y)$ is now given implicitly by

$$y = \frac{4\gamma}{(\gamma+1)}\left(\frac{\tilde{\delta}}{\tilde{H}}\right)\left[\frac{1}{2}\ln\left|\frac{z^2 \pm bz + c}{z_0^2 \pm bz_0 + c}\right| - \frac{b}{2d}F(z)\right], \tag{11.1}$$

$$F(z) = \begin{cases} \ln\left|\dfrac{2z+b-d}{2z+b+d}\dfrac{2z_0+b+d}{2z_0+b-d}\right|, & b^2 > 4c, \\ 2\left[\arctan\{(2z+b)/d\} - \arctan\{(2z_0+b)/d\}\right], & b^2 < 4c \end{cases} \tag{11.2}$$

$$b = \frac{2(\gamma-1)}{(\gamma+1)}B_i^*, \quad c = \left(\frac{8A_i^*}{(\gamma+1)M_0^2} - \frac{(3\gamma-1)}{(\gamma+1)}B_i^{*2}\right), \quad d = \sqrt{|b^2-4c|}. \tag{11.3}$$

It may be noted that in the formulae above A_i^* is yet to be determined; this is now done by forcing y to be 1 when $z = z_1$. This can only be done by iteration which, however, is considerably simplified by two observations. If the temperature profile is monotonic, as it indeed is in this case, A_i^* has, if $T_1 < 1$, to be greater than A_∞^*, the limiting value when $\tilde{\delta}/\tilde{H} \to 0$; if $T_1 > 1$, $A_i^* < A_\infty^*$. Secondly, from (8) it follows that $A_\infty^* = 1 + 0.5(\gamma-1)M_0^2$.

Figure 2*a* and *b* shows the temperature profiles for various values of the height parameter $\tilde{\delta}/\tilde{H}$ at a subsonic and a supersonic Mach number. We can see in both cases that the profiles are monotonic and that they are qualitatively not too different from the exponential profiles resulting from the linearized theory (Plesset 1952). The differences are naturally more pronounced at small $\tilde{\delta}/\tilde{H}$, when convection predominates over conduction, and large M_0, when nonlinear effects are expected to become more important. Figure 2*c* shows the effect of varying the Mach number M_0 for a fixed $\tilde{\delta}/\tilde{H} = 0.1$. Notice that the profiles depart non-monotonically from the exponential profile at low M_0 to a near linear profile around $M_0 = 1$ and to an exponential profile again at high M_0. This phenomenon is connected again with the behaviour in the neighbourhood of the critical Mach number, $M_{\mathrm{cr}} = 1/\sqrt{\gamma}$. An important difference between the linearized and the present nonlinear solutions is that the velocity and pressure are uniform in the former case but not so in the latter; this can be seen in figure 3.

PHILOSOPHICAL TRANSACTIONS OF THE ROYAL SOCIETY A MATHEMATICAL, PHYSICAL & ENGINEERING SCIENCES

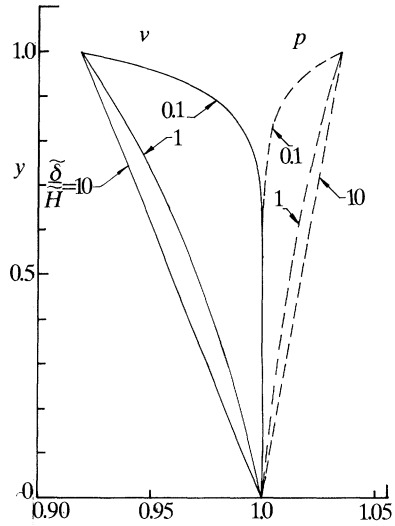

Figure 3. The velocity and pressure profiles at a Mach number $M_0 = 0.5$, $T_1 = 0.95$. Note that in the linearized case both velocity and pressure would be uniform.

It was pointed out when deriving (6) that for the purposes of the present analysis $1/\sqrt{\gamma}$ represented a critical Mach number. The physical explanation for its appearance follows from comparing the magnitude of the convection term in the energy equation (3.2) with the magnitude of the pressure work term. It is easy to show that they are in a ratio proportional to $(1-\gamma M^2)$ which vanishes as $M \to 1/\sqrt{\gamma}$ i.e. in the neighbourhood of M_{cr} pressure work dominates convection, irrespective of mass flux, and is balanced by conduction alone. The nature of this bifurcation can also be seen more clearly as follows. Since (5) together with (1.1) and (1.4) imply that the pressure is given by

$$p = 0.5\,\gamma M_0^2 [B_i^* \pm \sqrt{(B_i^{*2} - 4T/\gamma M_0^2)}] \tag{12}$$

and since the entropy for a perfect gas is given by

$$s = 1 + (\tilde{c}_p/\tilde{s}_0) \ln T - (\tilde{R}/\tilde{s}_0) \ln p \tag{13}$$

it is clear that for a given M_0 the temperature is a function of the entropy alone, independent of $\tilde{\delta}/\tilde{H}$ and $\tilde{T}_1/\tilde{T}_0$. Thus on a T–s diagram, as sketched in figure 4, for a given M_0 or mass flux the flow has a unique locus independent of $\tilde{\delta}/\tilde{H}$ and T_1. Equations (3.1) and (3.2) can also be combined to show that the following equation holds

$$\left(\frac{\tilde{\delta}}{\tilde{H}}\right)\frac{\mathrm{d}^2 T}{\mathrm{d}y^2} = \left\{\frac{1-M^2}{1-\gamma M^2}\right\}\frac{\mathrm{d}T}{\mathrm{d}y}, \tag{14}$$

where $M = M(y)$ is the local Mach number. It is now possible to show that if $M_0 < 1/\sqrt{\gamma}$ then $M(y) < 1/\sqrt{\gamma}$ and that if $M_0 > 1/\sqrt{\gamma}$, $M(y)$ has to be greater than $1/\sqrt{\gamma}$ i.e. M cannot equal $1/\sqrt{\gamma}$ in the interior of the field. In figure 4 this also implies that while T_1 can be greater or less than $T_0\,(=1)$ both have to be on the same side of the peak of the curve (corresponding to $M = 1/\sqrt{\gamma}$). Note too that the critical Mach number implies a maximum permissible T_1 given by

$$T_{1M} = 1 + (1-\gamma M_0^2)^2/4\gamma M_0^2. \tag{15}$$

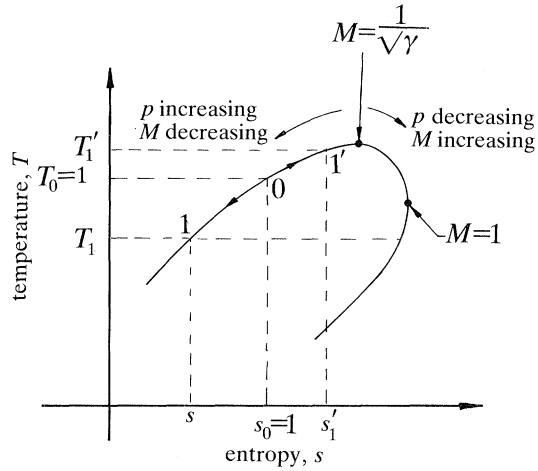

Figure 4. The locus of the gas dynamic flow on the T–s diagram for a given Mach number M_0. The point 0 corresponds to the lower surface, 1 to the upper surface when $T_1 < 1$ and 1′ to the upper surface when $T_1' > 1$.

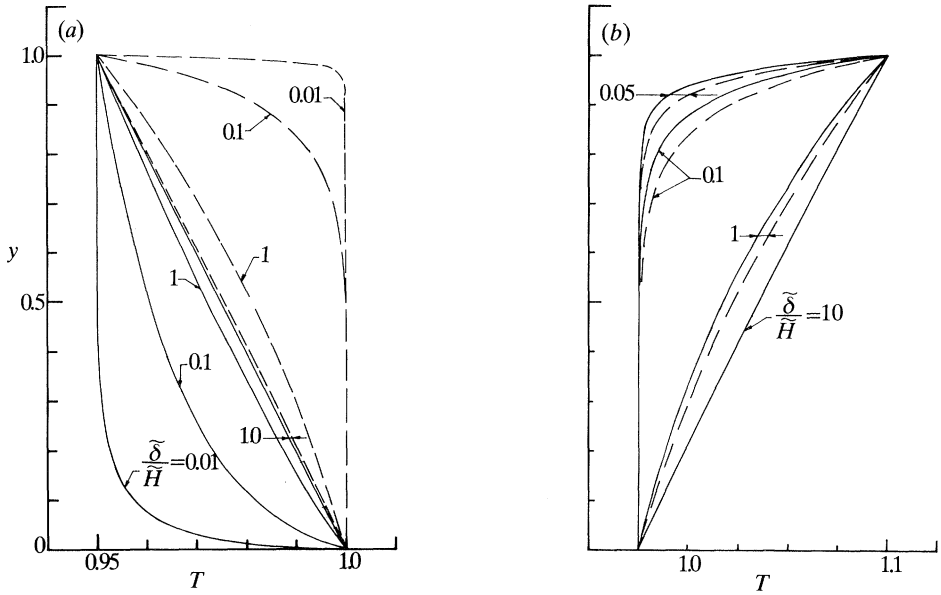

Figure 5. (*a*) Temperature profiles for a supercritical Mach number, $M_0 = 0.8$, $T_1 = 0.95$. Corresponding exponential profiles are shown by dotted lines. (*b*) Temperature profiles for a subcritical Mach number, $M_0 = 0.5$ with $T_1 > 1$. Corresponding exponential profiles are shown by dotted lines.

The unusual nature of the temperature profiles in the range $1/\sqrt{\gamma} < M_0 < 1$ is shown in figure 5*a*. The profiles are all concave (upwards) while for Mach numbers outside this range the temperature profiles are always convex as shown in figures 2 and 5*b*. In figure 5*b* the computations are for a case where $T_1 > 1$ (i.e. $\tilde{T}_1 > \tilde{T}_0$). It is to be emphasized that while $T_1 > 1$ corresponds in the evaporation problem to the anomalous temperature distribution case, in general both $T_1 < 1$ and $T_1 > 1$ are of interest. While our analysis is general and the frame work is non-dimensional, all the

computations in this paper are for mercury vapour around 100 °C, the case of greatest experimental importance (Shankar & Deshpande 1990*a*). For this reason γ has been taken to be $\frac{5}{3}$ for all the computations shown.

Using (10) and (14) we can prove the following assertions regarding the inviscid gas dynamic field.

1. Provided $T_1 < T_{1M}$ the solution exists for all $\tilde{\delta}/\tilde{H}$ and all M_0 except $M_0 = 1/\sqrt{\gamma}$. For $M_0 = 1/\sqrt{\gamma}$, T_1 has to be less than T_0 and one can in figure 4 descend either by the subcritical, decelerating (left) or supercritical, accelerating (right) path; however, while the solution exists for all heights on the accelerating path the height has to be less than a critical height on the decelerating path.
2. The temperature profile is always monotonic.
3. If $M_0 < 1/\sqrt{\gamma}$ the flow accelerates if $T_1 > 1$ and decelerates if $T_1 < 1$. The opposite hold if $M_0 > 1/\sqrt{\gamma}$.
4. It is not possible to accelerate or decelerate through the critical Mach number $M_{\mathrm{cr}} = 1/\sqrt{\gamma}$.
5. It is possible on the supercritical branch to accelerate or decelerate through the maximum entropy point, $M = 1$.

We shall conclude this discussion of the inviscid field by pointing out, in summary, that the nonlinear effects are mild and are important only for moderate M_0 and small $\tilde{\delta}/\tilde{H}$. A number of interesting features appear at the higher Mach numbers especially at and beyond $M_0 = 1/\sqrt{\gamma}$. We shall see, however, that the inclusion of viscosity completely changes the picture: even the qualitative features are totally different. Thus an inviscid model makes sense only for low or moderate Mach numbers.

4. The viscous solution: Prandtl number = 0.75

We shall now consider the role of viscosity in the gas dynamic field. Before considering the general case, we shall in this section consider the field for a gas with $Pr = 0.75$. This is motivated by the fact that in this case the hydrodynamic and thermal boundary layer thicknesses are of equal magnitude and as a consequence the energy equation can be integrated, as noted in the earlier shock structure investigations, to yield an expression for the total enthalpy. One is then left with a single nonlinear equation to solve for the velocity. From a practical point of view, the case is far from being artificial as most gases and vapours have Prandtl numbers in the range 0.7–1.0, e.g. mercury vapour, in the temperature range of interest to us, has a Prandtl number around 0.69 while water vapour has a Prandtl number close to 0.94. Thus the simplification is of genuine utility.

In order to obtain an explicit expression for the dimensionless total enthalpy $Q = T + 0.5(\gamma-1)M_0^2 v^2$, one first eliminates the pressure term in the energy equation (1.3) by using the momentum equation (1.2) to obtain

$$\frac{\mathrm{d}T}{\mathrm{d}y} + (\gamma-1)M_0^2 v\frac{\mathrm{d}v}{\mathrm{d}y} = \left(\frac{\tilde{\delta}}{\tilde{H}}\right)\frac{\mathrm{d}^2T}{\mathrm{d}y^2} + \tfrac{4}{3}(\gamma-1)M_0^2 Pr\left(\frac{\tilde{\delta}}{\tilde{H}}\right)\left(v\frac{\mathrm{d}^2v}{\mathrm{d}y^2} + \left(\frac{\mathrm{d}v}{\mathrm{d}y}\right)^2\right). \tag{16}$$

Now if $Pr = \frac{3}{4}$, the above expression can be immediately integrated to yield

$$Q(y) = T + 0.5(\gamma-1)M_0^2 v^2 = A^* + D\exp\{y/(\tilde{\delta}/\tilde{H})\}, \tag{17}$$

where the constants D and A^* are explicitly given by

$$D = \{(T_1-1) + 0.5(\gamma-1)M_0^2(v_1^2-1)\}/(\exp(\tilde{H}/\tilde{\delta})-1), \tag{18.1}$$

$$A^* = 1 + 0.5(\gamma-1)M_0^2 - D. \tag{18.2}$$

Equation (17) implies that the total enthalpy $Q(y)$ has an exponential profile across the field; (18.1) further implies that for small $\tilde{\delta}/\tilde{H}$ a boundary layer of thickness of order $\tilde{\delta}/\tilde{H}$ exists near the upper surface. To get a single equation for the velocity one first integrates the momentum equation to obtain

$$v = -(1/\gamma M_0^2)\, p + \tfrac{4}{3} Re^{-1}\, \mathrm{d}v/\mathrm{d}y + B^* \tag{19}$$

with B^* a constant (cf. B_i^* in the inviscid case) and $Re^{-1} = \frac{3}{4}\tilde{\delta}/\tilde{H}$ since $Pr = \frac{3}{4}$. Using (1.1), (1.4) and (17) we get the following equation for the velocity

$$\left(\frac{\tilde{\delta}}{\tilde{H}}\right) v \frac{\mathrm{d}v}{\mathrm{d}y} + B^* v - \frac{(\gamma+1)}{\gamma} v^2 = \frac{A^* + D \exp\,(y\tilde{H}/\tilde{\delta})}{\gamma M_0^2} = \frac{Q(y)}{\gamma M_0^2}. \tag{20}$$

Though the equation is of first order, two boundary conditions need to be satisfied: $v(0) = 1$, $v(1) = v_1$. This is indeed necessary as B^* is as yet unknown and its determination is akin to that of determining an eigenvalue. One may recall that in the inviscid case B_i^*, the total momentum flux, was an integral of the motion; as a consequence the locus of the flow lay on a prescribed trajectory in the T–s plane (figure 4). In the viscous case B^* is not an integral of the motion and depends in essence on the slope of the velocity at the lower boundary. Since the temperature is therefore not a function of the entropy alone, with the mass flux as a parameter, the gas dynamic flow has no simple trajectory in the T–s plane. Some of these complex trajectories, computed for the viscous case, are given in Shankar & Deshpande (1990*b*).

The innocuous looking nonlinear equation (20) does not appear to have a simple closed form solution and has in general to be solved numerically. For all the computations presented in this paper the procedure was as follows. An initial value of B^* was chosen and the equation integrated using an accurate Runge–Kutta scheme to give a value for $v(1)$. If $v(1)$ was not equal to v_1, the prescribed value, B^* was changed and the procedure repeated until $|v(1) - v_1|$ was sufficiently small. A reasonable starting value for B^* is $B_i^* = 1 + (\gamma M_0^2)^{-1}$; the direction in which to proceed is then suggested by (19) and the sign of $(v_1 - 1)$. Once B^* and $v(y)$ are determined T can be found from (17) after which all the other variables can be computed.

Figure 6*a*–*e* shows the results of computations carried out for $M_0 = 0.5$ and $T_1 = 0.95$. Figure 6*a* and *b* depicts the variation of velocity and temperature between the surfaces as a function of the height parameter $\tilde{\delta}/\tilde{H}$. The velocity decreases monotonically with y for all values of $\tilde{\delta}/\tilde{H}$; this appears to always be the case, as one might expect even when viscous forces are at play. For large $\tilde{\delta}/\tilde{H}$ the velocity is linear in y, as in the inviscid case; but for $\tilde{\delta}/\tilde{H} \to 0$ the velocity is uniform, at a value between v_1 and 1, over most of the field with boundary layers at either surface. The boundary layers become thinner as $\tilde{\delta}/\tilde{H} \to 0$. The temperature profiles shown in figure 6*b* are quite unexpected. For large $\tilde{\delta}/\tilde{H}$ the profiles are linear; but for $\tilde{\delta}/\tilde{H} \to 0$ the profiles are not monotonic and actually show a temperature overshoot. These viscous results immediately show a totally different qualitative and quantitative picture from the inviscid case. Again for $\tilde{\delta}/\tilde{H} \to 0$ the temperature takes a uniform value, greater than both T_1 and T_0 over most of the field with boundary layers around $y = 0, 1$. The Mach number profiles in figure 6*c* can be inferred from the behaviour of v and T. It may be recalled that in the inviscid case the upper pressure p_1 could not be specified arbitrarily; indeed p_1 was determined by the values chosen for M_0, $\tilde{\delta}/\tilde{H}$ and

PHILOSOPHICAL TRANSACTIONS OF THE ROYAL SOCIETY A MATHEMATICAL, PHYSICAL & ENGINEERING SCIENCES

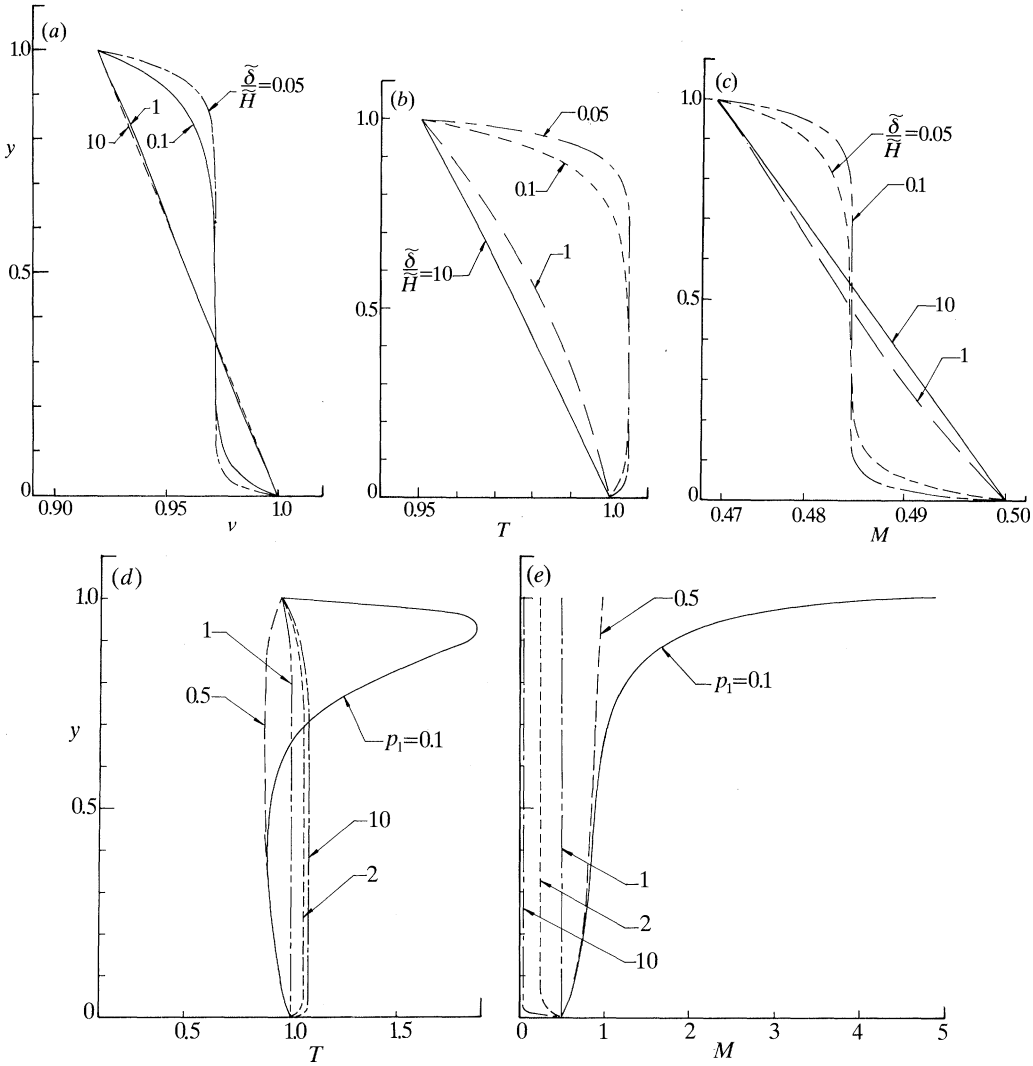

Figure 6. (*a*) The velocity profile as a function of $\tilde{\delta}/\tilde{H}$ for a fluid with Prandtl number 0.75. $M_0 = 0.5$, $T_1 = 0.95$ and $p_1 = p_{1i} = 1.0338$. (*b*) Temperature profiles for the same conditions as in (*a*). (*c*) Mach number profiles for the same conditions as in (*a*). (*d*) Temperature profiles in the vapour as affected by the pressure ratio. $Pr = 0.75, M_0 = 0.5, T_1 = 0.95$ and $\tilde{\delta}/\tilde{H} = 0.1$. (*e*) The Mach number distribution as affected by the pressure ratio for the same conditions as in (*d*).

T_1. Let us call this value of p_1, p_{1i}. So far the computations displayed in figure 6*a–c* were for $p_1 = p_{1i} = 1.0338$; in the subcritical inviscid flow of §3 a decreasing temperature is accompanied by compression. But the viscous field is not so limited and can accommodate other pressure ratios too. The variation of the temperature field with p_1 is shown in figure 6*d* for $M_0 = 0.5$, $T_1 = 0.95$ and $\tilde{\delta}/\tilde{H} = 0.1$. Once again the temperature profiles are counter intuitive: for pressure ratios greater than 1 a temperature overshoot occurs, for small pressure ratios a temperature undershoot occurs, while for still lower ratios the undershoot is followed by a very large overshoot. For $p_1 = 0.1$ the undershoot is just a little more than the applied temperature difference while the overshoot is about 18 times the applied gradient.

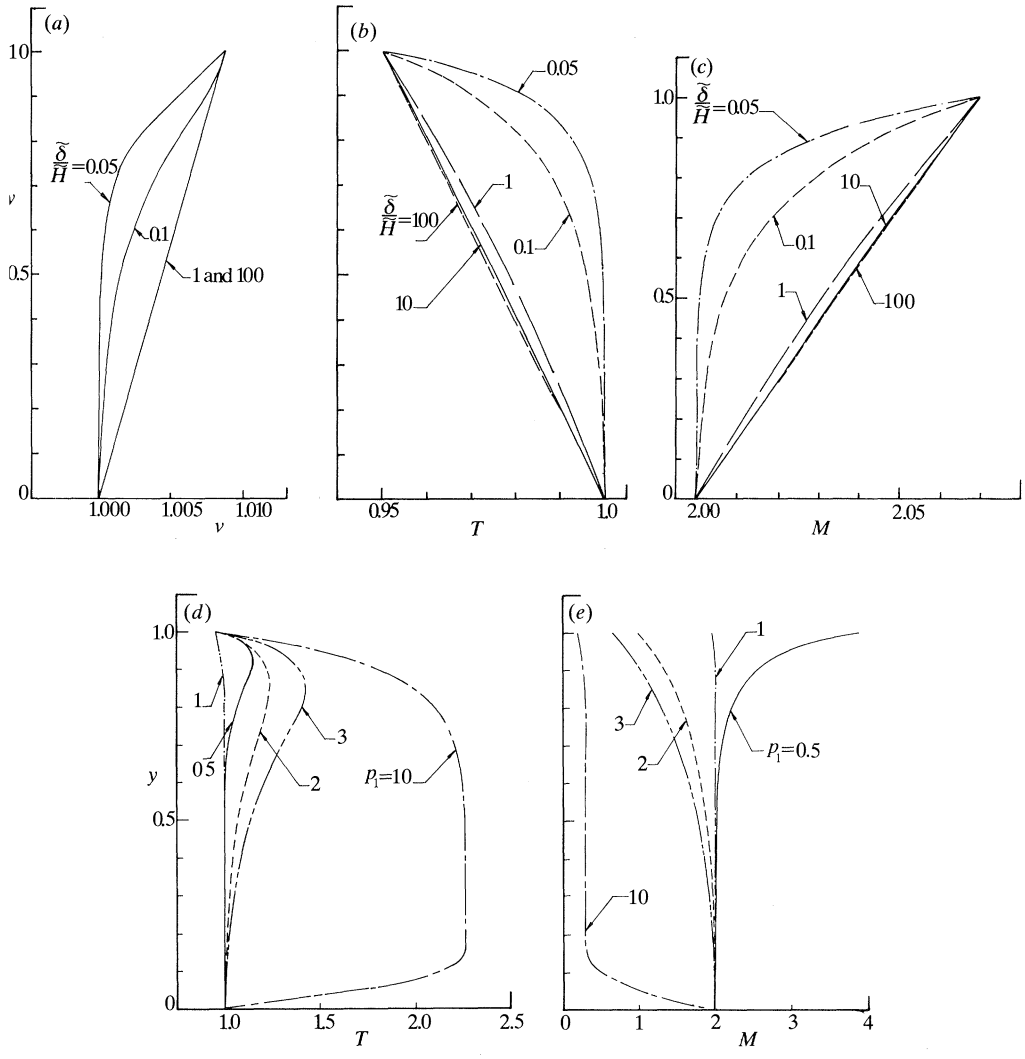

Figure 7. (*a*) The velocity profiles in the vapour for various values of $\tilde{\delta}/\tilde{H}$. $Pr = 0.75$, $M_0 = 2.0$, $T_1 = 0.95$, $p_1 = 0.94179 = p_{1i}$. (*b*) Temperature profiles in the vapour for the same conditions as in (*a*). (c) Mach number profiles for the same conditions as in (*a*). (*d*) The effect of the pressure ratio on the temperature profile. $Pr = 0.75$, $M_0 = 2.0$, $T_1 = 0.95$, $\tilde{\delta}/\tilde{H} = 0.1$. (*e*) Mach number profiles corresponding to the conditions in (*d*).

This is particularly surprising since the flow is accelerating in this case with the flow becoming supersonic around $y = 0.66$ and still the gas heats up instead of cooling. This is purely due to viscous dissipation. Finally figure 6*e* shows Mach number profiles as a function of p_1: large variations occur once p_1 is small enough for the flow to become supersonic.

Other than in some rare situations, in explosive ablation for example, supersonic values for M_0 are unlikely to be relevant to the phase change problem, especially as conceived till now. On the other hand in the general gas dynamic context in which we are interested, it is natural to inquire as to what happens when M_0 goes supersonic. Figure 7*a–e* shows the results of calculations done for a supersonic Mach

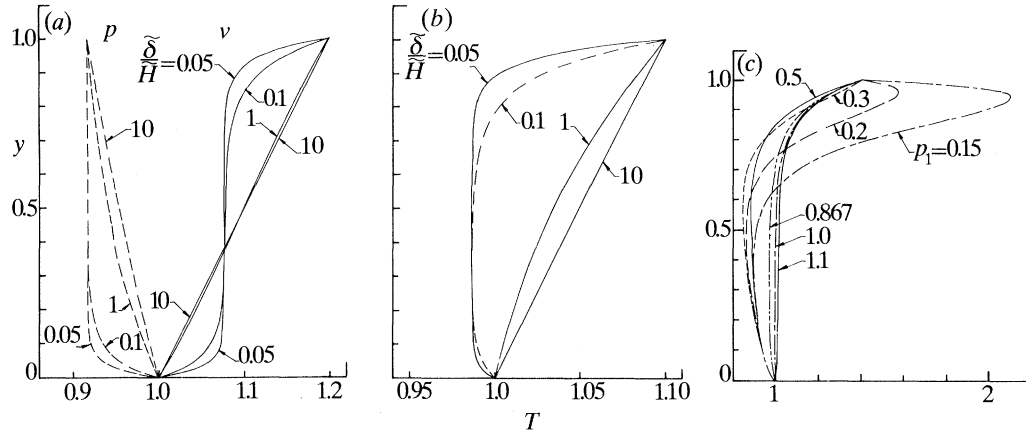

Figure 8. (*a*) The velocity and pressure fields as a function of $\tilde{\delta}/\tilde{H}$ for $Pr = 0.75, M_0 = 0.5, T_1 = 1.10, p_1 = 0.91668 = p_{1i}$. (*b*) The temperature field for the same conditions as in (*a*). (*c*) The effect of varying pressure ratio on the temperature profiles. $Pr = 0.75, M_0 = 0.5, \tilde{\delta}/\tilde{H} = 0.1, T_1 = 1.4$.

number $M_0 = 2.0$ with $T_1 = 0.95$. Figure 7*a–c* shows that the profiles are much closer to the inviscid solution than in the subsonic case. For the parameters shown , T and M are all monotonic in y for all the values of $\tilde{\delta}/\tilde{H}$ considered; the temperature suffers no undershoot or overshoot and the profiles are linear for $\tilde{\delta}/\tilde{H} \to \infty$. This was for $p_1 = p_{1i} = 0.94179$. If we let p_1 depart from this value the temperature profiles become most interesting as shown in figure 7*d*; large temperature overshoots occur for both smaller and larger values of p_1. For $p_1 = 10$ the overshoot is as much as 25 times the applied difference $(1 - T_1)$! One might conjecture that the large temperature rise through dissipation might be connected with the compression of the vapour. This is only partly confirmed by the Mach number profiles shown in figure 7*e*, as a significant temperature rise occurs for $p_1 = 0.5$ even though the vapour expands to a Mach number in excess of 3.9.

In figures 6 and 7 T_1 is less than 1 corresponding, in the phase change context, to a normal temperature distribution. The situation in the gas dynamic field, pertinent to an anomalous temperature distribution, is depicted in figure 8, where T_1 is greater than 1. The velocity and temperature fields are similar to those obtained for $T_1 < 1$. While p_1 was chosen to coincide with the inviscid value p_{1i} for purposes of comparison, there is in fact no real restriction. Note too that in principle $T_1 (> 1)$ is not restricted in the same way as in the inviscid case (see equation (15)).

The effect of varying the Mach number M_0 on the temperature distribution, for fixed $\tilde{\delta}/\tilde{H}, T_1$, etc., is shown in figure 9*a* and *b* for two values of p_1. In figure 9*a* $p_1 = p_{1i}$ for $M_0 = 0.5$, while in figure 9*b* $p_1 = p_{1i}$ for $M_0 = 2$; in the first figure the gas suffers compression while in the second it expands. Once again one is struck by the significantly different qualitative pictures. In figure 9*a* temperature overshoots of varying magnitude occur at all Mach numbers and $(\mathrm{d}T/\mathrm{d}y)_0 > 0$ at all but the lowest Mach numbers. In figure 9*b*, on the other hand, there are no temperature overshoots and $(\mathrm{d}T/\mathrm{d}y)_0 < 0$ for all Mach numbers. Equally significant is the S-shaped profile for $M_0 = 0.5$: profiles such as these have been observed experimentally (Shankar & Deshpande 1990*a*) a point to which we will return later.

Finally, figure 10*a* and *b* relates to a somewhat extreme situation where the temperatures in the fluid rise to almost unbelievable levels. The Mach number at the

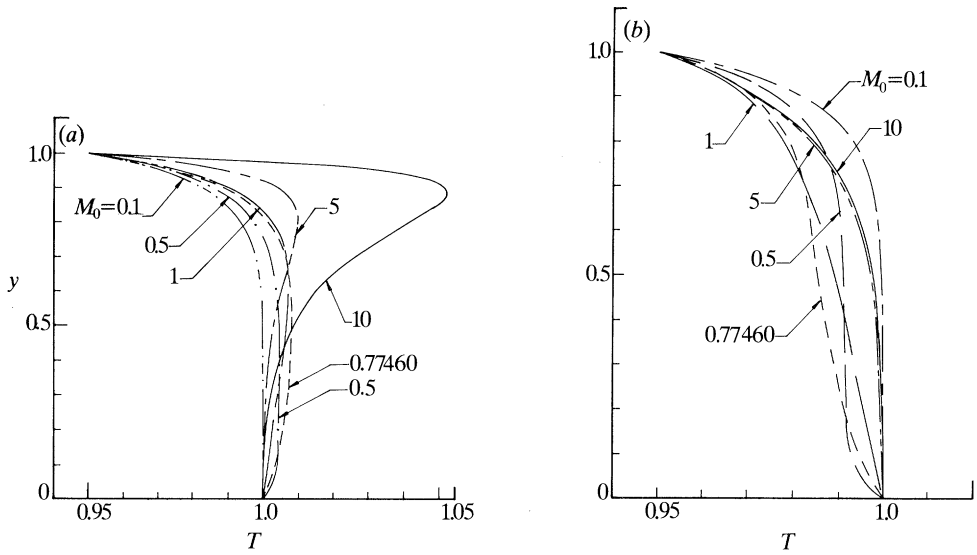

Figure 9. (*a*) The effect of varying the Mach number M_0 on the temperature distribution. The upper pressure $p_{1i} = 1.0338 = p_{1i}$ corresponding to $M_0 = 0.5$, $Pr = 0.75$, $T_1 = 0.95$, $\tilde{\delta}/\tilde{H} = 0.1$. (*b*) The effect, on the temperature distribution, of varying the Mach number M_0. The upper pressure $p_1 = 0.94179 = p_{1i}$ corresponding to $M_0 = 2.0$, $Pr = 0.75$, $T_1 = 0.95$, $\tilde{\delta}/\tilde{H} = 0.1$.

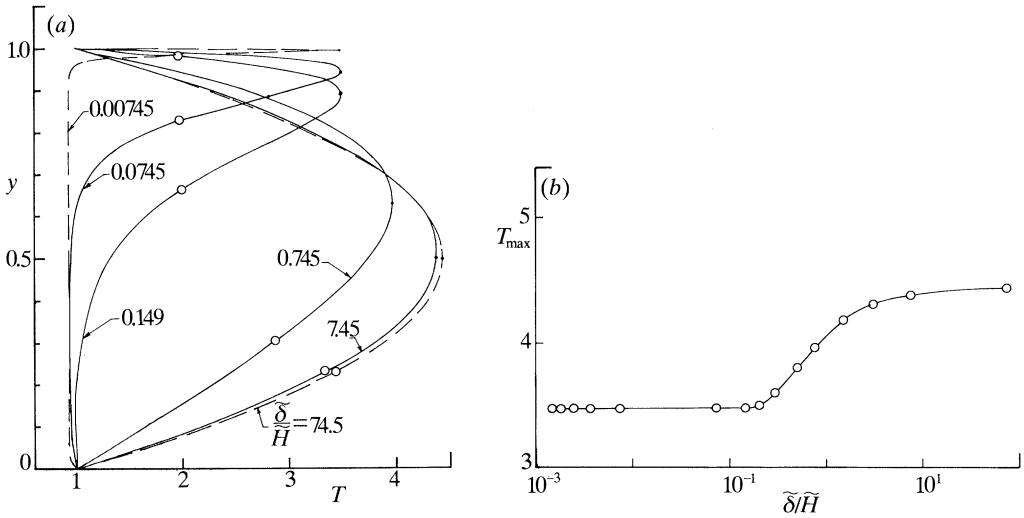

Figure 10. (*a*) Some remarkable temperature distributions corresponding to flows involving severe expansion. $Pr = 0.75$, $M_0 = 0.39261$, $T_1 = 0.94638$, $p_1 = 0.054348$. (*b*) The maximum temperature in the field as a function of $\tilde{\delta}/\tilde{H}$ for the data considered in (*a*).

lower surface is modest, less than 0.4, but the pressure ratio is sufficiently small ($p_1 \approx 0.05$) to force the upper Mach number M_1 to be greater than 7. The peak temperature ratio is greater than 3.4 (i.e. more than 65 times the applied temperature difference); as might be expected, since dissipation is likely to be greater for large $\tilde{\delta}/\tilde{H}$, the ratio is greater at large $\tilde{\delta}/\tilde{H}$. It must be noted that if $\tilde{T}_0 = 100$ °C the maximum temperature in the field will be in excess of 1000 °C! The magnitude of the viscous heating in the gas is quite astonishing and we feel that there are likely to be

Table 1. *The constants A* and B*; Pr = 0.75, $T_1 = 0.95$*

	$M_0 = 0.5$	$p_1 = 1.03376$	$M_0 = 2.0$	$p_1 = 0.94179$
$\tilde{\delta}/\tilde{H}$	A^*	B^*	A^*	B^*
0.05	1.083330	3.452976	2.333285	1.149990
0.10	1.083333	3.452979	2.333286	1.149911
0.50	1.093184	3.462356	2.337457	1.146214
1.0	1.119970	3.492771	2.348799	1.141581
5.0	1.367684	3.806860	2.453691	1.106465
10.0	1.681970	4.210678	2.586761	1.062858

other physical situations, perhaps in astrophysics, where such effects are likely to be actually seen. Figure 10*b* clearly suggests that limiting solutions are likely to exist for $\tilde{\delta}/\tilde{H} \to \infty$ and $\tilde{\delta}/\tilde{H} \to 0$. We shall derive these in the next subsections, but first present table 1 which lists values of the constants A^* and B^* as functions of $\tilde{\delta}/\tilde{H}$ for a particular set of values for M_0, T_1 and p_1. Note again that limiting values for the constants are suggested for $\tilde{\delta}/\tilde{H} \to 0$; in the other limit they appear to increase linearly. We now take up these asymptotic analyses.

4.1. *The solution for small heights* ($\tilde{\delta}/\tilde{H} \to \infty$)

All the examples in the previous subsection suggest that an asymptotic solution exists for $\tilde{\delta}/\tilde{H} \to \infty$, or for small heights. On physical grounds one would expect the velocity, in this limit, to be linear in y and the solutions presented so far suggest the correctness of this idea.

For $\tilde{\delta}/\tilde{H} \to \infty$ the total enthalpy $Q(y)$ given by (17), has the expansion

$$Q(y) = Q_0 - (Q_0 - Q_1)\, y + (1/2\chi)(Q_0 - Q_1)(y - y^2) + O(\chi^{-2}), \tag{21}$$

where $\chi = \tilde{\delta}/\tilde{H}$, is the height parameter. Equation (20) for the velocity may then be written

$$\chi v \frac{\mathrm{d}v}{\mathrm{d}y} + B^* v - \frac{(\gamma+1)}{\gamma} v^2 = \frac{1}{\gamma M_0^2}\left[\{Q_0 - \Delta Q y\} + \frac{1}{2\chi}\{\Delta Q (y - y^2)\}\right] + O(\chi^{-2}), \tag{22}$$

where $\Delta Q = Q_0 - Q_1$. Now assume that the velocity has, for $\chi \to \infty$, an expansion of the form

$$v = u^{(0)} + \chi^{-1} u^{(1)} + \chi^{-2} u^{(2)} + \ldots. \tag{23}$$

All the computational results suggest a linear form for the leading term

$$u^{(0)} = 1 - (1 - v_1)\, y, \tag{24}$$

which satisfies the boundary conditions. The leading term in the expansion for B^* is then suggested by (22)

$$B^* \approx \chi B^{*(-1)} = \chi(1 - v_1). \tag{25}$$

Equations (24) and (25) constitute the solution to leading order for $\chi \to \infty$. To get the first-order correction we substitute the above forms into (22) to get the equation relevant to order $\chi^0 (= 1)$

$$u^{(0)}\, \mathrm{d}u^{(1)}/\mathrm{d}y + \{\mathrm{d}u^{(0)}/\mathrm{d}y + B^{*(-1)}\} = (Q_0 - \Delta Q y) + [(\gamma+1)/2\gamma]\, u^{(0)^2} - B^{*(0)} u^{(0)}. \tag{26}$$

It is to be noted that $B^{*(0)}$ is yet to be determined and that the term in curly brackets

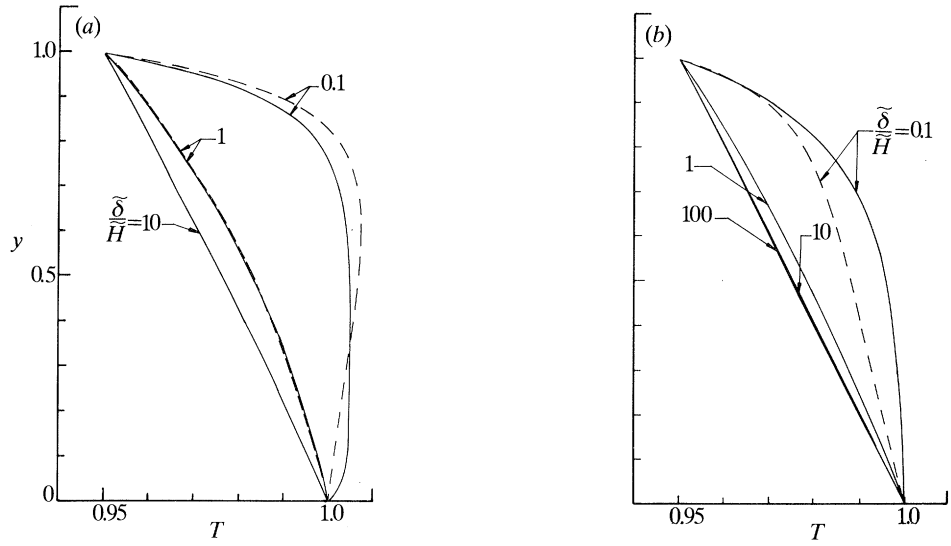

Figure 11. (*a*) Comparison of the temperature profiles as predicted by the asymptotic theory for large $\tilde{\delta}/\tilde{H}$ with the 'exact' solution. – – –, Equations (27, 17); ——, 'exact' solution. $Pr = 0.75$, $M_0 = 0.5$, $T_1 = 0.95$, $p_1 = 1.0338$. (*b*) As in (*a*). – – –, Equations (27, 17); ——, 'exact' solution. $Pr = 0.75$, $M_0 = 2.0$, $T_1 = 0.95$, $p_1 = 0.94179$.

is identically zero. Equation (26) can easily be integrated and the boundary conditions used to determine $B^{*(0)}$. We therefore obtain to order χ^{-1} in the velocity, the following solution as $\chi \to \infty$

$$v(y) = \{1-(1-v_1)\} + \chi^{-1}\left[\frac{\Delta Q}{\Delta v}\frac{1}{\gamma M_0^2}\left\{y + \left(\frac{1}{\Delta v} - \frac{Q_0}{\Delta Q}\right)(\ln|1-\Delta v y|)\right\} + 0.5((\gamma+1)/\gamma)\,(y - \tfrac{1}{2}\Delta v y^2) - B^{*(0)} y\right], \quad (27.1)$$

$$B^* = \chi\,\Delta v + \left[\frac{\Delta Q}{\Delta v}\frac{1}{\gamma M_0^2}\left\{1 + \left(\frac{1}{\Delta v} - \frac{Q_0}{\Delta Q}\right)(\ln|1-\Delta v|)\right\} + \frac{(\gamma+1)}{2\gamma}(1 - \tfrac{1}{2}\Delta v)\right], \quad (27.2)$$

where $\Delta v = 1 - v_1$ and $\Delta Q = Q_0 - Q_1$. The temperature is of course given by (17) and the above. Figure 11*a* and *b* clearly shows that the asymptotic solutions derived above for $\tilde{\delta}/\tilde{H} \to \infty$ are excellent approximations for $\tilde{\delta}/\tilde{H}$ values as low as 1 for the subsonic case and as low as 0.1 in the supersonic case. Naturally the B^* values also check but we refrain from giving the data.

4.2. *Asymptotic analysis for large heights* ($\tilde{\delta}/\tilde{H} \to 0$)

We have seen from all the computational results presented so far that when $\tilde{\delta}/\tilde{H} \to 0$ the flow quantities become uniform over most of the field with boundary layers near both the surfaces. In order to derive the flow field in this limit let us assume that when $\chi = \tilde{\delta}/\tilde{H} \to 0$, v has the expansion

$$v = u^{(0)} + \chi u^{(1)} + O(\chi^2). \quad (28)$$

As we shall only derive the leading-order term $u^{(0)}$ we shall in what follows drop the superscript zero. Since in this limit

$$Q(y) = Q_0 + \Delta Q\,(1 - e^{y/\chi})/(e^{1/\chi} - 1) = Q_0 + O(e^{-1/\chi})$$

except in the neighbourhood of $y = 1$, equation (20) for the velocity reduces to

$$\chi u\,\mathrm{d}u/\mathrm{d}y + B^* u - [(\gamma+1)/2\gamma]\,u^2 = Q_0/\gamma M_0^2. \tag{29}$$

Thus the total enthalpy over most of the field is constant and equal to the value at the lower surface. Now if we let $\chi \to 0$ in (29), the derivative term disappears giving the classical indication that we have a singular perturbation problem on hand and that inner expansions will have to be derived to complete the solution. No matter we conclude that over most of the field the velocity is constant, i.e. $u = v_\infty$, and given by

$$B^* v_\infty - [(\gamma+1)/2\gamma]\,v_\infty^2 = Q_0/\gamma M_0^2, \tag{30.1}$$

$$v_\infty = \{\gamma/(\gamma+1)\}[B^* \pm \sqrt{\{B^* - 2((\gamma+1)/\gamma)\cdot Q_0/\gamma M_0^2\}}]. \tag{30.2}$$

Observe that B^* is yet to be determined. To determine B^* we construct inner expansions around $y = 0$ and 1 and match them to the outer solution (30); matching, however, does not lead to the determination of B^*. This is achieved by inserting the solutions into an integral identity and solving the resulting equation for B^*. If we integrate (20) from $y = 0$ to $y = 1$ we obtain the exact relation

$$I = \int_0^1 \left\{B^* v - \frac{(\gamma+1)}{2\gamma} v^2\right\} \mathrm{d}y = -\tfrac{1}{2}\chi\{v_1^2 - 1\} + \frac{\{Q_0 + \Delta Q(\mathrm{e}^{1/\chi} - 1)^{-1}\}}{\gamma M_0^2} - \frac{\chi\,\Delta Q}{\gamma M_0^2}. \tag{31}$$

To derive the inner expansion around $y = 0$ we set $\eta = y/\chi$ as the inner variable and obtain for the leading term v_{i0} of the inner expansion the equation

$$v_{i0}\,\mathrm{d}v_{i0}/\mathrm{d}\eta + B v_{i0} - [(\gamma+1)/2\gamma]\,v_{i0}^2 = Q_0/\gamma M_0^2. \tag{32}$$

Unfortunately the left-hand side of (32) contains the nonlinear operator of the full equation. We therefore obtain an approximate solution by assuming an exponential form for v_{i0} and choosing the exponent so that the differential equation is satisfied at $\eta = 0$, i.e.

$$v_{i0} = v_\infty + (1 - v_\infty)\exp(-\alpha_0 \eta), \tag{33.1}$$

$$\alpha_0 = \{B^* - 1 - (\gamma M_0^2)^{-1}\}/(1 - v_\infty). \tag{33.2}$$

Note that B^* and v_∞, the uniform velocity in the outer field, are still to be determined. Similarly, instead of attempting to solve the inner equation around $y = 1$, we assume an exponential form for the leading term v_{i1} of that inner expansion and choose the exponent so that the equation is satisfied at $\eta_1 = (1-y)/\chi = 0$, i.e.

$$v_{i1} = v_\infty + (v_1 - v_\infty)\exp(-\alpha_1 \eta_1), \tag{34.1}$$

$$\alpha_1 = \{-B^* + v_1 + (T_1/\gamma M_0^2 v_1)\}/(v_1 - v_\infty). \tag{34.2}$$

It may be observed that both forms chosen satisfy the boundary conditions and the equation at their respective boundaries and smoothly match the uniform field as $\eta, \eta_1 \to \infty$.

The velocity fields given by (33), (30) and (34) are now substituted into the left side of the integral equation (31) to obtain a second relation between v_∞ and B^* in addition to (30.1). These can then be solved (see Shankar & Deshpande 1990*b* for details) to yield the approximate solution

$$v_\infty = 1 + \nu \quad (\nu \ll 1), \tag{35.1}$$

$$B^* = B_0^* + b = \{1 + (\gamma M_0^2)^{-1}\} + b \quad (b \ll 1), \tag{35.2}$$

PHILOSOPHICAL TRANSACTIONS OF THE ROYAL SOCIETY A MATHEMATICAL, PHYSICAL & ENGINEERING SCIENCES

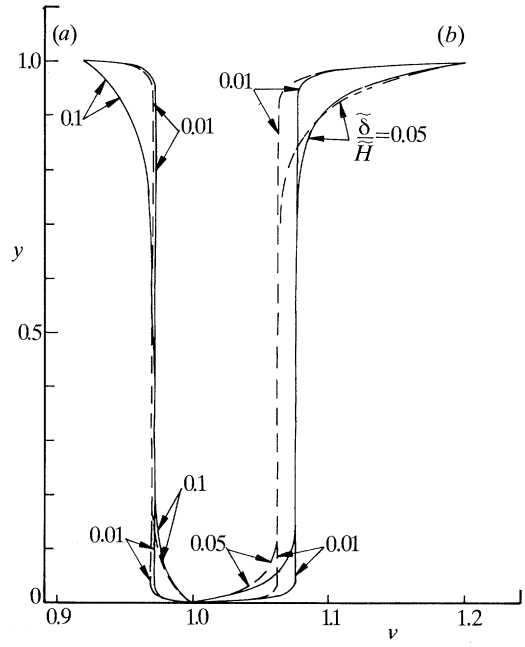

Figure 12. Comparison of the velocity profiles as predicted by the asymptotic theory for small $\tilde{\delta}/\tilde{H}$ with the 'exact' solution. – – –, Equation (36); ——, 'exact' solution. $Pr = 0.75$, $M_0 = 0.5$; (*a*) $T_1 = 0.95$, $p_1 = 1.0337$; (*b*) $T_1 = 1.1$, $p_1 = 0.91668$.

where

$$\left.\begin{aligned}
k_0 &= (M_0^2-1)/\gamma M_0^2, \quad k_1 = \{2+(\gamma-1)M_0^2\}/2\gamma M_0^2, \quad k_2 = B_0^* - v_1 - (T/\gamma M_0^2 v_1),\\
f_0 &= -[\Delta T/M_0^2 - (1-v_1^2)/2]/\gamma,\\
N &= f_0 k_0 k_2 + \{B_0^* k_0 - ((\gamma+1)/4\gamma) k_0 (v_1+3)\}(\Delta v)^2,\\
D_1 &= B_0^*\{k_2 - 2k_0\Delta v - k_1(\Delta v)^2\} - k_0^2(\Delta v)^2 - f_0(k_0^2 + k_1 k_2),\\
D_2 &= ((\gamma+1)/4\gamma)\{4k_2 - 2k_0(3+v_1)\Delta v - (3k_0 + k_1(3+v_1))(\Delta v)^2\},\\
\nu &= N/(D_1 - D_2), \quad b = (k_0 + k_1\nu)\nu.
\end{aligned}\right\} \tag{36}$$

The above approximate solution for $\tilde{\delta}/\tilde{H} \to 0$ explicitly shows the complex dependence of the uniform velocity field ($v_\infty = 1+\nu$) on the five parameters M_0, $\tilde{\delta}/\tilde{H}$, γ, v_1 and T_1. When $\tilde{\delta}/\tilde{H} \to 0$ we know that convection is predominant with conduction of importance only near the boundaries. Thus one expects the velocity and temperature to take on uniform values, close to the lower surface values, over most of the field with rapid changes in a thin boundary layer near the upper surface. Indeed in the inviscid case of §3 the uniform values are exactly equal to the lower surface values as $\tilde{\delta}/\tilde{H} \to 0$. When viscosity is present the uniform value for the velocity v_∞ is close to 1 but not equal to 1; in fact $v_1 < v_\infty < 1$ or $1 < v_\infty < v_1$. The dependence on all the parameters is complex but it is quite possible, as has been shown, for the flow to be cooled below the upper and lower surface temperatures. Cooling can take place in spite of dissipation.

Finally, figure 12 shows some velocity profiles computed using (33)–(36) for some typical values of the parameters. It is remarkable, considering all the approximations made, how good the agreement is in figure 12*a*; it is not so good in figure 12*b* mainly

Table 2. *The variation of A^* and B^* with Prandtl number; $\tilde{\delta}/\tilde{H} = 0.25$*

	$M_0 = 0.5$, $T_1 = 0.95$, $p_1 = 1.03376$		$M_0 = 0.5$, $T_1 = 1.4$, $p_1 = 0.2$	
Pr	A^*	B^*	A^*	B^*
0	1.083694	3.400083	—	—
0.10	1.082841	3.411418	1.109188	3.177964
0.20	1.082608	3.420627	1.116836	3.055302
0.25	1.082625	3.424657	1.114318	3.013119
0.30	1.082700	3.428390	1.109577	2.974362
0.40	1.082970	3.435144	1.095181	2.897867
0.50	1.083346	3.441154	1.075025	2.816822
0.60	1.083784	3.446591	1.049388	2.728805
0.70	1.084261	3.451576	1.018525	2.633358
0.75	1.084508	3.453927	1.001243	2.582922
0.80	1.084760	3.456197	0.982791	2.530759
0.90	1.085273	3.460523	0.942607	2.421584
1.00	1.085793	3.464607	0.898416	2.306500

because ν is not sufficiently small to justify the approximations made. Suggestions for better approximations are made in Shankar & Deshpande (1990*b*).

5. The viscous solution for arbitrary Prandtl number

We now consider the general case of the flow of a vapour with arbitrary Prandtl number. The momentum and energy equations (1.2) and (1.3) can both be integrated once to give the pair of coupled nonlinear equations

$$\left(Pr\frac{\tilde{\delta}}{\tilde{H}}\right)\frac{\mathrm{d}v}{\mathrm{d}y} = \frac{3}{4}\left[\frac{1}{\gamma M_0^2}\frac{T}{v} + v - B^*\right], \tag{37.1}$$

$$(\tilde{\delta}/\tilde{H})\,\mathrm{d}T/\mathrm{d}y = [T/\gamma - \tfrac{1}{2}(\gamma-1)M_0^2 v^2 + (\gamma-1)M_0^2 B^* v - A^*], \tag{37.2}$$

where B^* and A^* are constants to be determined. Observe that when the Prandtl number vanishes (37.1) reduces to the integrated inviscid momentum equation (5). As before four boundary conditions, namely $v_0 = T_0 = 1$, $v(1) = v_1$, $T(1) = T_1$, are available to determine the two integration constants and A^* and B^*.

The solution procedure is as follows. Initial values are guessed for A^* and B^*; using these, equations (37) are integrated using an accurate Runge–Kutta scheme to yield values for $v(1)$ and $T(1)$. If $|v(1)-v_1|$ and $|T(1)-T_1|$ are not sufficiently small A^* and B^* are changed appropriately until convergence to the desired boundary values is achieved. Efficiency is achieved by carefully choosing the initial values and by using a generalized Newton–Raphson technique to hunt for the 'eigenvalues'. Table 2 shows how A^* and B^* vary with Prandtl number for a given choice of the other parameters. Note that when $T_1 = 0.95$ the pressure ratio chosen, $p_1 = 1.03376$, corresponded to the inviscid pressure ratio p_{1i} and so the constants A^* and B^* tend to their inviscid values A_i^* and B_i^* as $Pr \to 0$. For the other case shown, $p_1 = 0.2 \neq p_{1i}$ and so a comparison with the inviscid result is not possible.

One may observe from figure 13*a* how the temperature profile changes as the Prandtl number is varied in the range $0.1 \leqslant Pr \leqslant 1.0$. We are not concerned with Prandtl numbers greater than 1 since our interest is limited to gases and vapours. In

PHILOSOPHICAL TRANSACTIONS OF THE ROYAL SOCIETY A MATHEMATICAL, PHYSICAL & ENGINEERING SCIENCES

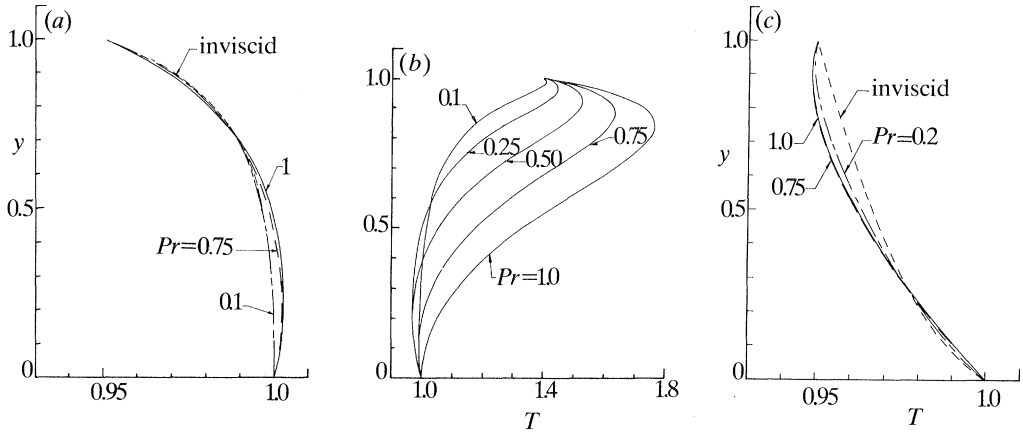

Figure 13. (*a*) The effect of Prandtl number on the temperature profile. $M_0 = 0.5$, $T_1 = 0.95$, $p_1 = 1.03376$, $\tilde{\delta}/\tilde{H} = 0.25$. (*b*) The effect of Prandtl number on the temperature profile. $M_0 = 0.5$, $T_1 = 1.4$, $p_1 = 0.2$, $\tilde{\delta}/\tilde{H} = 0.25$. (*c*) The temperature profile as affected by the Prandtl number. $M_0 = 0.8$, $T_1 = 0.95$, $p_1 = 0.8$, $\tilde{\delta}/\tilde{H} = 0.25$.

the higher range of Prandtl numbers the temperature overshoot phenomenon is apparent. As the Prandtl number is reduced the profiles smoothly merge to the inviscid profile (corresponding to $Pr = 0$), where there is no overshoot. Note that in this case $p_1 = p_{1i}$. In figure 13*b* the upper pressure corresponds to a case forbidden by the inviscid model. Note that the temperature overshoot decreases in magnitude as $Pr \to 0$, presumably because viscous heating is less severe. Figure 13*c* shows the effect of Prandtl number in a case that would be considered supercritical in the inviscid limit. Note the undershoots in the viscous cases and the persistence of viscous effects at as low a Prandtl number as 0.2.

We now briefly examine the behaviour of the solutions in the general case when $\chi = \tilde{\delta}/\tilde{H} \to \infty, 0$. For the limit of small heights or $\chi \to \infty$ we assume the following forms as suggested by the analysis of §4.1,

$$v = v^{(0)} + \chi^{-1} v^{(1)} + \dots, \tag{38.1}$$

$$T = T^{(0)} + \chi^{-1} T^{(1)} + \dots, \tag{38.2}$$

$$B^* = \chi B^{*(-1)} + B^{*(0)} + \dots, \tag{38.3}$$

$$A^* = \chi A^{*(-1)} + A^{*(0)} + \dots. \tag{38.4}$$

If these forms are substituted into equations (37) the solution to leading order is found to be

$$v^{(0)}(y) = 1 - \Delta v y, \tag{39.1}$$

$$T^{(0)}(y) = 1 + \{\tfrac{2}{3}(\gamma-1) M_0^2 Pr(\Delta v)^2 - \Delta T\} y - \tfrac{2}{3}(\gamma-1) M_0^2 Pr(\Delta v)^2 y^2, \tag{39.2}$$

$$B^{*(-1)} = \tfrac{4}{3} Pr(1 - v_1), \tag{39.3}$$

$$A^* = \tfrac{4}{3}(\gamma-1) M_0^2 Pr\{\Delta v - 0.5(\Delta v)^2\} + \Delta T, \tag{39.4}$$

where $\Delta v = 1 - v_1$ and $\Delta T = 1 - T_1$. These solutions are quite interesting in that while the velocity profile is linear irrespective of the Prandtl number the temperature is strongly influenced by the parameter. When $Pr \to 0$ the temperature profile is linear exactly as in the inviscid case; but otherwise the temperature profile is quadratic in y as shown in figure 10*a*. This surprising result is again entirely due to the effect of

viscosity in the fluid. Note that if the temperature attains a maximum in the field, it will in this limit be given by

$$T_{\max} = 1 + \frac{\{\frac{2}{3}(\gamma-1)M_0^2 Pr(\Delta v)^2 - \Delta T\}}{4(\frac{2}{3}(\gamma-1))M_0^2 Pr(\Delta v)^2}. \tag{40}$$

If the parameters pertaining to figure 10*a* are inserted into the formula above, the peak temperature is estimated very accurately. As regards the limit $\chi \to 0$, we know that in both the inviscid and $Pr = \frac{3}{4}$ cases the velocity and temperature are uniform over most of the field. In the inviscid case the uniform values taken correspond to the lower surface values with a boundary layer near the top; in the $Pr = \frac{3}{4}$ case boundary layers exist near both surfaces. This suggests that in (37), when $\chi \to 0$ the left hand side should be dropped. Thus if v_∞ and T_∞ are the constant values for velocity and temperature over most of the field, they have to satisfy

$$(\gamma M_0^2)^{-1} T_\infty / v_\infty + v_\infty + B^* = 0, \tag{41.1}$$

$$T_\infty/\gamma - 0.5(\gamma-1)M_0^2 v_\infty^2 + (\gamma-1)M_0^2 v_\infty B^* - A^* = 0. \tag{41.2}$$

It should be noted that B^* and A^* are functions of Prandtl number. To proceed we need as in §4.2 to develop matching inner expansions and then use two integral equations. This can be done but we shall not proceed here in this direction.

6. Discussion

We have seen in the foregoing the very considerable effects of nonlinearity and dissipation on the gas dynamic field in liquid–vapour phase change. Nonlinearity alone leads to results that are quantitatively different from the commonly used linearized inviscid calculations but are not qualitatively very different; some qualitative differences do exist, especially for higher Mach numbers, but they may not be very important practically. Viscosity on the other hand produces dramatic changes both qualitative and quantitative. Through the action of viscous normal stresses and dissipation the temperature profile, which is monotonic in an inviscid fluid, can suffer overshoots or undershoots, whose magnitude can be very large indeed. For small values of the height parameter $\tilde{\delta}/\tilde{H}$, the viscous field has narrow boundary layers at both boundaries, whereas the inviscid field has a boundary layer only at the top; both fields are uniform outside the boundary layers. For large values of the height parameter the temperature profile is, surprisingly, quadratic in y when viscosity is present rather than linear as when it is absent. In addition to these striking qualitative differences the quantitative differences can also be very large depending on the values of the parameters such as M_0, $\tilde{\delta}/\tilde{H}$, p_1, etc.

It might be appropriate at this point to recall an interesting circumstance that arose in the inviscid situation. It was found then that $M_0 = 1/\sqrt{\gamma}$ represented a critical Mach number; it was not possible to accelerate or decelerate through this Mach number. Moreover, unlike in a subcritical or supersonic flow, the temperature profile was concave upwards. What happens in the viscous field? To answer this one must try to find an equivalent to (14) of §3. It is possible by combining the energy equation with the momentum equation to obtain a relation of the type

$$(\tilde{\delta}/\tilde{H})\,\mathrm{d}^2T/\mathrm{d}y^2 = (1-\gamma M^2)^{-2} F(M, M', M'', T').$$

Whereas in the inviscid case (14) implied the impossibility of the Mach number

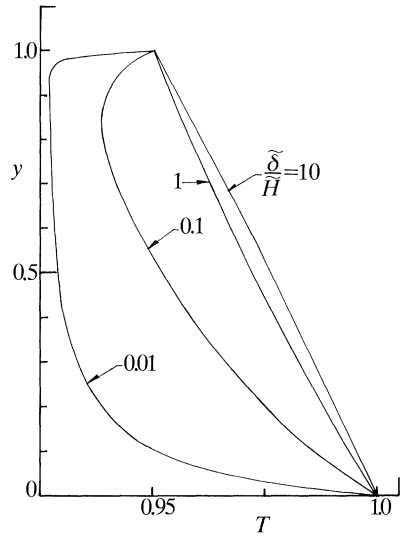

Figure 14. The effect on the temperature profile of varying the height parameter $\tilde{\delta}/\tilde{H}$ in a transcritical case. $Pr = 0.75$, $M_0 = 0.8$, $T_1 = 0.95$, $p_1 = 0.8$.

being $1/\sqrt{\gamma}$ in the interior of the field, the above equation shows that singularities need not arise if $F = 0$ when $M(y)$ equalled $1/\sqrt{\gamma}$. This, indeed, is the case and it is quite possible for a viscous flow to negotiate M_{cr} in the interior of the field. As regards the nature of the temperature profiles in the transcritical case the situation is complex as is illustrated in figure 14. For $\tilde{\delta}/\tilde{H} = 10$ the curve is convex upwards unlike the situation normally obtained in transcritical cases; for small $\tilde{\delta}/\tilde{H}$, however, the curves are concave with large temperature undershoots. The role of viscosity is indeed complex.

The principal motivation for the current analysis has been the potential application to the condensation–evaporation problem. A successful procedure used so far in tackling the problem has been one in which the continuum, inviscid gas dynamic equations are assumed to apply over most of the field with gas kinetic effects confined to Knudsen layers adjacent to the liquid surfaces (Aoki & Cercignani 1983; Shankar 1988). So far such approaches have involved linearization and have neglected viscous normal stress effects and dissipation. Without solving the full phase change problem, which we have not done so far, we wish now to see what implications, if any, the present nonlinear, viscous analysis would have on the latter approaches. For purposes of comparison we have used equations (5) and (6) of Aoki & Cercignani (1983) to compute the jumps and the linearized profile; the pressure ratio p_1 has been computed using the inviscid (nonlinear) analysis. Figure 15*a* and *b* are now to be compared with figure 2 of Aoki & Cercignani. It may now be recalled that the non-dimensional parameter $\beta = \tilde{L}/\tilde{R}\tilde{T}_0 - 1$, where $\tilde{L}$ is the latent heat, arises naturally in the linearized analysis of phase change. By Trouton's rule β takes the value 9 for all liquids but in reality the parameter normally takes on much larger values, e.g. for water $\beta \approx 18$–20 and for mercury $\beta \approx 20$–22 in our range of interest. Figure 15*a* corresponds to a somewhat low value of 6 for β only to permit comparison with figure 2 of Aoki & Cercignani; figure 15*b* deals with the realistic value of 20 for β. In figure 15*a* the nonlinear effects are small but the viscous effects, though small, change the qualitative picture by permitting the temperature undershoot. In figure 15*b*, whose

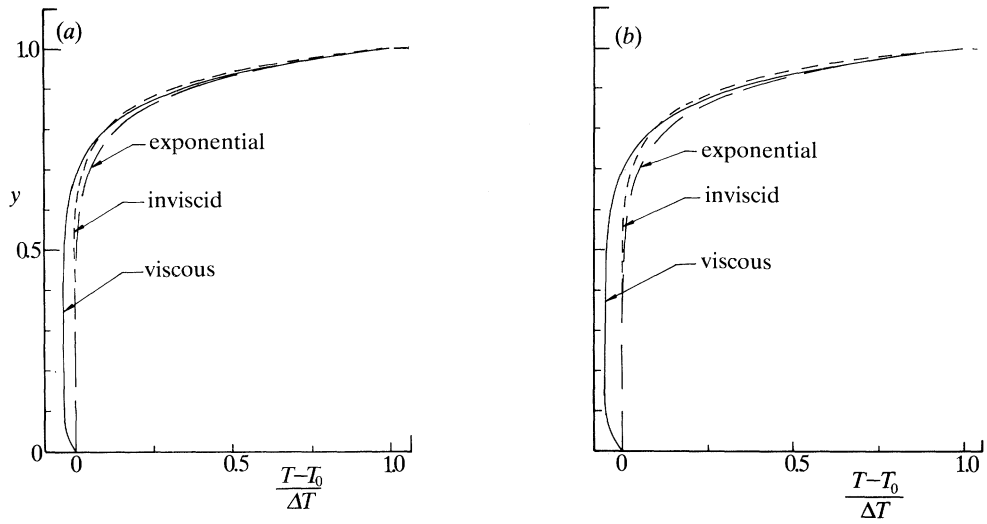

Figure 15. (*a*) The effects of nonlinearity and viscosity on the gas dynamic temperature field in liquid–vapour phase change. –––, Linearized analysis (Aoki & Cercignani 1983); - - - - -, inviscid, nonlinear; ——, viscous. $Pr = 0.75$, $M_0 = 0.4$, $\tilde{\delta}/\tilde{H} = 0.1$, $T_1 = 1.1$, $p_1 = p_{1i} = 0.96164$. (*b*) The effects of nonlinearity and viscosity on the gas dynamic temperature field in liquid–vapour phase change. –––, Linearized analysis (Aoki & Cercignani 1983); - - -, inviscid nonlinear; ——, viscous. $Pr = 0.75$. $M_0 = 0.4$, $\tilde{\delta}/\tilde{H} = 0.1$, $T_1 = 1.3$, $p_1 = p_{1i} = 0.86666$.

β value is realistic and close to that of mercury and most other vapours, the temperature undershoot is even more pronounced. Choosing a larger M_0 and smaller $\tilde{\delta}/\tilde{H}$ would, naturally, lead to even greater discrepancies. We must point out once again that we have yet to solve the full phase change problem; the above data only show that nonlinear and viscous effects are bound to be of very great significance.

Finally one might ask whether the temperature profiles predicted here have been observed experimentally? It is an unfortunate fact that very few experiments have been performed in this area. Reliable experiments are difficult to perform because one has to work at low densities, avoid contamination of the liquid surfaces and the vapour, etc.; further, for the effects to be large one needs to have γ as high as possible. The only experiments that we are aware of are our own (Deshpande & Shankar 1988) using mercury as the working fluid. Figure 16 shows a comparison of some data from those experiments with a theoretical calculation assuming certain values of the parameters M_0, $\tilde{\delta}/\tilde{H}$, etc. All that we wish to show is that it is possible to compute a viscous field temperature profile which has the same S-shaped character as the experimental data; note that no choice of parameters could lead to such a shape from an inviscid analysis, linear or nonlinear! The present work also shows the importance of also measuring the velocity field in any experiment: this is a difficult task but if done would help to make detailed comparisons with the theory possible.

We have said nothing here on the question of the anomalous temperature distribution predicted by the linearized theories of condensation and evaporation. Unless the coupling of the gas dynamic field to the Knudsen layers is completed it would be premature to predict anything on this issue. It is clear from the present analysis, however, that the assumption that the pressure is constant is likely to be a poor one and this is bound to affect the computation of the temperature

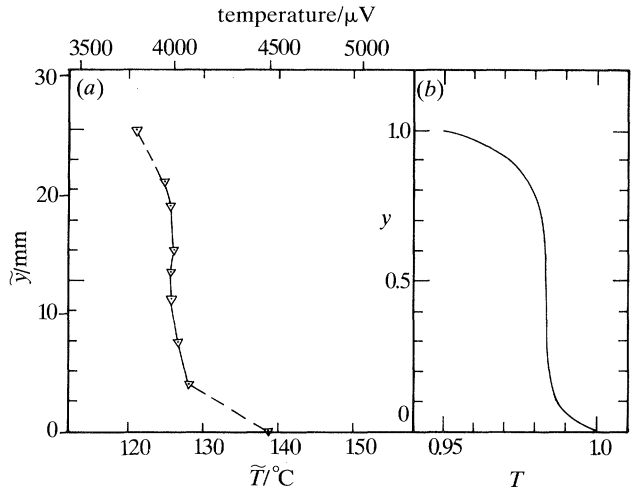

Figure 16. A qualitative comparison of some experimental data and a theoretical temperature distribution. (*a*) The experimental data are taken from Deshpande & Shankar (1988). (*b*) The theoretical distribution is for $Pr = 0.75$, $M_0 = 0.5$, $\tilde{\delta}/\tilde{H} = 0.1$, $T_1' = 0.95$ and $p_1 = 0.9$.

distribution. Both the magnitude of the temperature jumps and the temperature distribution itself are likely to be strongly influenced by viscous effects, especially in massive phase change. The present analysis in fact shows that the temperature distribution can be even more peculiar than had hitherto been imagined. But detailed analysis including that of the Knudsen layers has still to be done to confirm this.

7. Conclusion

We have shown in this paper that nonlinearity and viscosity can have large, if not dramatic effects, on the gas dynamic field in liquid–vapour phase change. The principal results are that the temperature profile can admit a non-monotonic behaviour with undershoots and overshoots and that the temperature peaks can be large. It is possible that the spectacularly large peaks, predicted by the theory for some values of the parameters, may never actually be achieved in practice because of practical limitations. However, it is difficult not to speculate on the possibility that these extreme results may be relevant to other related areas of investigation, e.g. astrophysics. Quantitative aspects apart, it is now clear that at least qualitatively the role of viscosity has so far been vastly underestimated. We are confident that many of the remarkable predictions of the present theory will in due course be confirmed by more careful experiments than have so far been performed.

References

Aoki, K. & Cercignani, C. 1983 Evaporation and condensation on two parallel plates at finite Reynolds numbers. *Phys. Fluids* **26**, 1163.

Cercignani, C., Fiszdon, W. & Frezzoti, A. 1985 The paradox of the inverted temperature profiles between an evaporating and a condensing surface. *Phys. Fluids* **28**, 3237.

Deshpande, M. D. & Shankar, P. N. 1988 Experiments on liquid–vapour phase change between plane liquid surfaces. Part 3, NAL Tech. Memo TM FM 8809.

Koffman, L. D., Plesset, M. S. & Lees, L. 1984 Theory of evaporation and condensation. *Phys. Fluids* **27**, 876.

PHILOSOPHICAL TRANSACTIONS OF THE ROYAL SOCIETY A MATHEMATICAL, PHYSICAL & ENGINEERING SCIENCES

Matsushita, T. 1976 Kinetic analysis of the problem of evaporation and condensation. *Phys. Fluids* **19**, 1712.

von Mises, R. 1950 On the thickness of a steady shock wave. *J. aero. Sci.* **17**, 551.

Morduchow, M. & Libby, P. A. 1949 On the complete solution of the one-dimensional flow equations of a viscous, heat-conducting, compressible gas. *J. aero. Sci.* **16**, 674.

Onishi, Y. 1986 The spherical-droplet problem of evaporation and condensation in a vapour–gas mixture. *J. Fluid Mech.* **163**, 171.

Pao, Y. P. 1971 Application of kinetic theory to the problem of evaporation and condensation. *Phys. Fluids* **15**, 306.

Plesset, M. S. 1952 Note on the flow of vapour between plane liquid surfaces. *J. chem. Phys.* **20**, 790.

Plesset, M. S. & Prosperetti, A. 1976 Flow of vapour in a liquid enclosure. *J. Fluid Mech.* **78**, 433.

Shankar, P. N. 1970 A kinetic theory of steady condensation. *J. Fluid Mech.* **40**, 385.

Shankar, P. N. 1988 Liquid–vapour phase change between plane liquid surfaces: a continuum analysis to determine real gas effects. NAL Tech. Memo TM FM 8803.

Shankar, P. N. & Deshpande, M D. 1990*a* On the temperature distribution in liquid–vapour phase change between plane liquid surfaces. *Phys. Fluids* A **2**, 1030.

Shankar, P. N. & Deshpande, M. D. 1990*b* Viscous and non-linear effects in the gas dynamics of phase change. NAL Tech. Memo TM CF 9001.

Received 2 October 1990; accepted 14 November 1990

PHILOSOPHICAL TRANSACTIONS OF THE ROYAL SOCIETY A MATHEMATICAL, PHYSICAL & ENGINEERING SCIENCES